Inorg. Chem. **2007**, *46*, 2224–2236

Functional Tetrametallic Linker Modules for Coordination Polymers and Metal–Organic Frameworks

Frank B. Johansson, Andrew D. Bond, and Christine J. McKenzie*

Department of Physics and Chemistry, University of Southern Denmark, Campusvej 55, 5230 Odense M, Denmark

Received November 10, 2006

The new biphenol-based tetranucleating ligand, 2,2′,6,6′-tetrakis(*N*,*N*-bis(2-pyridylmethyl)aminomethyl)-4,4′-biphenolate, $dbpbp^{2-}$, comprises two linearly disposed phenolato-hinged dinucleating heptadentate units, each of which offer one O and three N donors to a total of four metal ions. The ligand has been isolated as the zinc chloride complex $[Zn_4(dbpbp)Cl_4]^{2+}$, and the Zn^{II} ions have been completely or partially substituted by Cu^{II}, Fe^{III}, Co^{II}, and Co^{III} in metathesis reactions. Similarly, the chloride ligands of $[Zn_4(dbpbp)Cl_4]^{2+}$ have been exchanged for solvent molecules (acetonitrile and/or water) and bridging carboxylate ligands. The resulting complexes have been characterized by single-crystal X-ray diffraction, ESI mass spectrometry (ESI-MS), cyclic voltammetry (CV), and EPR spectroscopy. The structures containing $[M_4(dbpbp)Cl_4]^{2+}$ with M = Zn^{II} or Cu^{II} exhibit 2-D polymeric honeycomb sheets in which intermolecular M···Cl interactions bridge between adjacent $[M_4(dbpbp)Cl_4]^{2+}$ cations. Two mixed-metal tetrabenzoate complexes $[M_4(dbpbp)(O_2CC_6H_5)_4]^{2+/3+}$ have also been prepared, namely a stoichiometric $Cu^{II}_2Zn^{II}_2$ complex and a nonstoichiometric Fe^{III}/Zn^{II} system. In the latter case, ESI-MS identifies $FeZn_3$, Fe_2Zn_2, and Zn_4 species, and X-ray crystallography suggests an average composition of $Fe_{0.8}Zn_{3.2}$. Preparation of a Co^{II}_4 complex by metathesis was considerably more difficult than preparation of $[Cu_4(dbpbp)Cl_4]^{2+}$, requiring both a large excess of the cobalt source and the presence of auxiliary benzoate. In the presence of 2 equiv of benzoate per starting $[Zn_4(dbpbp)Cl_4]^{2+}$ unit and excess Co^{II}, dioxygen binds as peroxide at each end of the molecule to give the Co^{III}_4 complex $[Co_4(dbpbp)(O_2)_2(O_2CC_6H_5)_2]^{4+}$. This latter complex, together with new tetra- and hexametallic benzenedicarboxylato- and benzenetricarboxylato-bridged complexes of dinuclear $[Co_2(O_2)(bpbp)]^{3+}$ units ($bpbp^-$ = 2,6-bis(*N*,*N*-bis-(2-pyridylmethyl)aminomethyl)-4-*tert*-butyl-phenolate), is a module for potential construction of 1-D and 2-D coordination polymers/metal–organic frameworks (MOFs) capable of reversible O_2 binding.

Introduction

Coordination polymers and metal−organic frameworks (MOFs) are often synthesized by self-assembly reactions of relatively simple hydrated transition-metal or lanthanide cations with functionalized organic linkers that contain appropriately disposed coordinating groups such as carboxylate, cyanide, or pyridine.[1] The resulting materials can exhibit high porosity, gas absorptivity, and/or interesting magnetic, electronic, or optical properties,[2] all of which are potentially important characteristics for new functional materials. However, metal-ion precursors often have different coordination environments and properties in solution compared to the solid state, making it difficult to predict and control the chemical and topological properties of derivative coordination polymers/MOFs. Some degree of topological control has been gained by reticular synthesis, whereby the use of rigid and preformed molecular modules leads to heightened control in the assembly process and imparts particular properties to the modules. This ideology has been used, for example, by Robson[3] and others[4] to make porphyrin-based MOFs.

* To whom correspondence should be addressed. E-mail: chk@ifk.sdu.dk. Phone: +45 6550 2518. Fax: +45 6615 8780.

(1) (a) Yaghi, O. M.; Davis, C. E.; Li, G.; Li, H. *J. Am. Chem. Soc.* **1997**, *119*, 2861. (b) Yaghi, O. M.; Li, H.; Groy, T. L. *J. Am. Chem. Soc.* **1996**, *118*, 9096. (c) Yaghi, O. M.; O'Keeffe, M.; Ockwig, N. W.; Chae, H. K.; Eddaoudi, M.; Kim, J. *Nature* **2003**, *423*, 705. (d) Cussen, E. J.; Claridge, J. B.; Rosseinsky, M. J.; Kepert, C. J. *J. Am. Chem. Soc.* **2002**, *124*, 9574. (e) Chui, S. S.-Y.; Lo, S. M.-F.; Charmant, J. P. H.; Orpen, A. G.; Williams, I. D. *Science* **1999**, *283*, 148. (f) Pan, L.; Adams, K. M.; Hernandez, H. E.; Wang, X.; Zheng, C.; Hattori, Y.; Kaneko, K. *J. Am. Chem. Soc.* **2003**, *125*, 3062.

(2) (a) Kumagai, H.; Chapman, K. W.; Kepert, C. J.; Kurmoo, M. *Polyhedron* **2003**, *22*, 1921. (b) Kahn, O. *Acc. Chem. Res.* **2000**, *33*, 647.

10.1021/ic062131s CCC: $37.00
Published on Web 02/22/2007

Within this field, we have an interest in preparing functional MOFs that can take advantage of the cooperative effects of metal ions in close proximity. Such cooperativity is known from the active sites of numerous dinuclear metalloenzymes, for example the dioxygen carriers hemerythrin and hemocyanin, in which metal ions are found 2−4 Å from each other. As is typical for metalloenzyme active sites, and for substrate-activating catalysts in general, flexible metal coordination geometries, vacant coordination sites, and/or labile exchangeable ligands are essential for chemical reactivity. However, it is exactly these features that pose considerable challenges for the controlled production of MOFs, and coordinative flexibility or exchangeable ligands are therefore not commonly exploited for MOF construction. More predictable multinuclear nodal units such as dimetallic tetracarboxylate paddlewheel complexes, and tetrametallic basic hexacarboxylate units, have been incorporated into compounds such as Cu−BTC,[5] MOF-2,[6] and MOF-5,[7] and these materials have shown remarkable gas absorption properties. In these cases, however, the lack of readily accessible metal coordination sites presumably prevents direct interaction between the adsorbed molecules and the metal centers, and it is thus physisorption, rather than chemisorption, that best describes the gas−MOF interactions. Chemisorption of H_2 has been reported for iron-containing zeolites,[8] and nickel-containing phosphates,[9] where accessible coordinatively unsaturated iron and nickel centers provide the key for reactivity. These systems in particular suggest that nanoporous MOFs with accessible metal centers are promising targets for new functional materials.

This paper describes our first steps toward the construction of MOFs using tetrametallic linear linker modules that contain dimetallic sites with proven chemical reactivity. The ultimate aim is to realize a porous solid material that can reversibly bind dioxygen. To this end, we have prepared the new biphenol-based tetranucleating ligand, 2,2′,6,6′-tetrakis-(*N*,*N*-bis(2-pyridylmethyl)aminomethyl)-4,4′-biphenolate, $dbpbp^{2-}$ (Figure 1). The ligand is a covalently linked linear tail-to-tail dimer of the heptadentate phenolate-hinged ligand 2,6-bis(*N*,*N*-bis(2-pyridylmethyl)aminomethyl)-4-alkyl-phenolate ($bpmp^-$, alkyl = methyl;[10] $bpbp^-$, alkyl = *tert*-butyl[11]), which we and others have used previously to prepare dinuclear complexes, including mixed-metal and mixed-valence systems. Some of these dinuclear complexes have shown reactivity in the promotion of alkylester[11] and phosphate[12] hydrolysis reactions. More significantly in the present context, the dicobalt complexes of $bpbp^-$ have been shown to be capable of reversible dioxygen binding.[13] The crystal structure of the peroxo-bridged Co^{III}_2 cation $[Co_2(bpbp)(O_2)(O_2CCH_3)]^{2+}$ shows that the O_2-derived adducts exhibit 6-coordination at each Co^{III} center.[13a] On removal of dioxygen, the system is reduced to Co^{II}_2, which can then take up O_2 again, both in the solid state and in solution. The exact geometry of the reduced Co^{II}_2 complex is yet to be verified by crystallographic analysis, but the fact that O_2 uptake occurs in solution without a marked solvent dependence (even in the presence of coordinating solvents such as water, acetonitrile, methanol, or DMF) suggests that solvent coordination/decoordination is not involved, and that the Co^{II} ions in the reduced state are most likely 5-coordinate. In addition, the fact that the process occurs reversibly in the solid state suggests that the geometrical rearrangement is not large. Thus, the $dbpbp^{2-}$ system is an excellent candidate for incorporation into our envisaged functional coordination polymer/MOF. With this aim in mind, we describe here the preparation and characterization of several tetrametallic complexes of $dbpbp^{2-}$ that are suitable to act as linker modules for MOF construction, including the Co^{III}_4 system that can reversibly bind dioxygen. We also demonstrate the feasibility of linking these modules via linear benzene dicarboxylate (BDC) and trigonal benzene tricarboxylate (BTC) bridging groups. The collection of complexes represents a feasible set of building blocks for construction of coordination polymers/MOFs incorporating functional dimetallic sites.

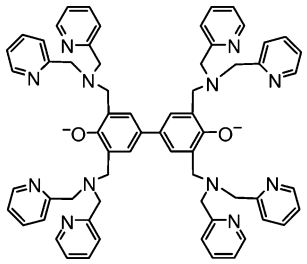

Figure 1. 2,2′,6,6′-Tetrakis(*N*,*N*-bis(2-pyridylmethyl)aminomethyl)-4,4′-biphenolate, $dbpbp^{2-}$.

Experimental Section

All chemicals were used as received from commercial suppliers. Elemental analyses were preformed at the Chemistry Department II, University of Copenhagen, Denmark. IR spectra were obtained from KBr discs using a Hitachi 27030 IR spectrometer. UV−vis spectra were obtained in CH_3CN (Sigma Aldrich, HPLC grade) at 25 °C using a Shimadzu UV-1601PC spectrometer equipped with a Shimadzu CPS-240A thermoelectrical temperature-controlled cell holder. Cyclic voltammetry was performed in a dry N_2-filled glovebox with an Autolab Potentionstat (Eco Chemie) connected to a standard three-electrode cell (platinum disk as working,

(3) Abrahams, B. F.; Hoskins, B. F.; Michail, D. M.; Robson, R. *Nature* **1994**, 369, 727.
(4) Goldberg, I. *Chem. Commun.* **2005**, *10*, 1243.
(5) Chui, S. S.-Y.; Lo, S. M.-F.; Charmant, J. P. H.; Orpen, A. G.; Williams, I. D. *Science* **1999**, 1148.
(6) Eddaoudi, M; Li, H.; Yaghi, O. M. *J. Am. Chem. Soc.* **2000**, *122*, 1391.
(7) Li, H.; Eddaoudi, M.; O'Keeffe, M.; Yaghi, O. M. *Nature* **1999**, *402*, 276.
(8) Mojet, B. L.; Eckert, J.; van Santen, R. A.; Albinati, A.; Lechner, R. E. **2001**, *123*, 8147.
(9) Forster, P. M.; Eckert, J.; Chang, J.-S.; Park, S.-E.; Ferey, G.; Cheetham, A. K. *J. Am. Chem. Soc.* **2003**, *125*, 1309.
(10) Suzuki, M.; Kanatomi, H.; Murase, I. *Chem. Lett.* **1981**, 1745.
(11) Ghiladi, M.; McKenzie, C. J.; Meier, A.; Powell, A. K.; Ulstrup, J.; Wocadlo, S. *J. Chem. Soc., Dalton Trans.* **1997**, 4011.
(12) (a) Seo, J. S.; Hynes, R. C.; Williams, D.; Chin, J.; Sung, N. D. *J. Am. Chem. Soc.* **1988**, *120*, 9943. (b) Seo, J. S.; Sung, N.-D.; Hynes, R. C.; Chin, J. *Inorg. Chem.* **1996**, *35*, 7472.
(13) (a) Ghiladi, M.; Gomez, J. T.; Hazell, A.; Kofod, P.; Lumtscher, J.; McKenzie, C. J. *J. Chem. Soc., Dalton Trans.* **2003**, 1320. (b) Wackerbarth, H.; Larsen, F. B.; Hansen, A. G.; McKenzie, C. J.; Ulstrup, J. *Dalton Trans.* **2006**, 3438.

Table 1. Selected Crystallographic Data for **1**−**6**, **8**, and **9**

	1[a]	**2**·2CH_3CN	**3**·CH_3CN	**3**[a]	**4**·2CH_3CN
formula	$[C_{64}H_{60}Cl_4Zn_4N_{12}O_2]$ $[Zn_2Cl_6]$[b]	$[C_{70}H_{71}N_{15}O_3Zn_4]$ $(ClO_4)_6$·2(CH_3CN)	$[C_{64}H_{60}Cl_4Cu_4N_{12}O_2]$ $[Zn_2Cl_6]$·CH_3CN	$[C_{64}H_{60}Cl_4Cu_4N_{12}O_2]$ $[Zn_2Cl_6]$[b]	$[C_{92}H_{80}Cu_2N_{12}O_{10}Zn_2]$ $[C_{14}H_{10}Cl_4O_4Zn_2]$·2$CH_3CN$
fw	1775.96	2110.71	1809.69	1768.64	2368.37
cryst syst	monoclinic	triclinic	monoclinic	monoclinic	triclinic
space group	*I*2/*m*	$P\bar{1}$	*I*2/*m*	*I*2/*m*	$P\bar{1}$
Z	2	1	2	2	1
T (K)	180(2)	180(2)	150(2)	150(2)	180(2)
a (Å)	11.7529(9)	10.8272(7)	11.869(3)	11.869(3)	11.0806(7)
b (Å)	27.090(2)	11.1926(7)	27.292(5)	27.292(5)	12.5195(8)
c (Å)	12.0596(9)	18.8464(11)	12.241(4)	12.241(4)	19.8843(13)
α (deg)	90	99.661(1)	90	90	97.482(3)
β (deg)	106.345(2)	100.107(1)	105.34(3)	105.34(3)	96.817(3)
γ (deg)	90	102.150(1)	90	90	98.501(3)
V (Å^3)	3684.4(5)	2147.8(2)	3823.9(17)	3823.9(17)	2678.0(3)
D_x (g cm^{-3})	1.601	1.632	1.572	1.536	1.469
λ (Å)	0.7107	0.7107	0.8970	0.8970	0.7107
μ (mm^{-1})	2.335	1.379	2.110	2.107	1.440
$2\theta_{max}$	49.8	52.7	63.8	63.8	53.0
no. reflns	9892	13612	5658	5658	48838
no. unique reflns/R_{int}	3282/0.055	8712/0.033	3142/0.065	3142/0.067	10817/0.068
no. obsd ($I > 2\sigma(I)$)	1925	5871	1898	1859	6393
R1 (obsd data)	0.058	0.066	0.095	0.069	0.057
wR2 (all data)	0.162	0.190	0.304	0.195	0.149
GOF on F^2	0.94	1.03	1.07	0.95	1.04
CCDC no.	625168	625169	625170		625171

	5	**6**[b]	**8**·4$(CH_3)_2CO$·8H_2O	**9**·6$(CH_3)_2CO$
formula	$[C_{92}H_{80}Fe_{0.8}N_{12}O_{10}Zn_{3.2}]$ $[B(C_6H_5)_4]_{2.8}$	$[C_{92}H_{80}Co_4N_{12}O_{10}]$ $[B(C_6H_5)_4]_2$[b]	$[C_{80}H_{82}Co_4N_{12}O_{10}](ClO_4)_4$·4 $(CH_3)_2CO8H_2O$	$[C_{117}H_{120}Co_6N_{18}O_{15}](ClO_4)_6$·6 $(CH_3)_2CO$
fw	2661.33	2387.82	2381.54	3317.06
cryst syst	monoclinic	triclinic	monoclinic	cubic
space group	$P2_1/c$	$P\bar{1}$	$P2_1/c$	$P2_13$
Z	2	2	2	4
T (K)	180(2)	180(2)	180(2)	180(2)
a (Å)	20.834(3)	19.191(9)	18.9268(8)	25.1232(11)
b (Å)	26.036(3)	19.763(6)	12.7196(5)	25.1232(11)
c (Å)	15.4807(18)	20.328(9)	21.7486(9)	25.1232(11)
α (deg)	90	83.299(9)	90	90
β (deg)	108.322(4)	66.759(6)	92.960(2)	90
γ (deg)	90	81.316(8)	90	90
V (Å^3)	7971.8(17)	6989(5)	5228.8(4)	15857.1(12)
D_x (g cm^{-3})	1.109	1.135	1.513	1.389
λ (Å)	0.7107	0.7107	0.7107	0.7107
μ (mm^{-1})	0.603	0.524	0.817	0.797
$2\theta_{max}$	41.6	41.6	46.9	45.9
no. reflns	61921	39471	65669	81624
no. unique reflns/R_{int}	8303/0.129	14472/0.096	7556/0.088	7265/0.060
no. obsd ($I > 2\sigma(I)$)	4586	7051	5107	5545
R1 (obsd data)	0.114	0.068	0.077	0.088
wR2 (all data)	0.372	0.173	0.245	0.270
GOF on F^2	1.05	0.86	1.05	1.05
Flack param				−0.03(4)
CCDC no.	625172	625173	625174	625175

[a] Refinement based on continuous solvent area model (*SQUEEZE*[15]). [b] Empirical formula is an estimate (see text).

platinum rod as counter, and 0.01 M $Ag/AgNO_3$ in 0.1 M tetra-*n*-butylammonium perchlorate (TBAP) in CH_3CN as reference electrode). Electrolyte solution was prepared from dry CH_3CN (LAB-SCAN, acetonitrile DNA anhydroscan, <10 ppm H_2O) with 0.1 M TBAP (Fluka, electrochemical grade) as supporting electrolyte. The ferrocenium/ferrocene ($Fc^{+/0}$) redox couple was measured to 0.09 V versus the reference electrode. All potentials are given versus $Fc^{+/0}$. EPR spectra were obtained at 116 K using a Bruker ESP-380E FTEPR spectrometer operating at 9.4 GHz (X-band) with 100 kHz modulation. Simulated spectra were calculated using the *SIM* program package.[14] Electrospray ionization mass spectra (ESI-MS) were recorded on a Finnigan TSQ 700 MAT triple quadrupole instrument equipped with a Finnigan API nanoelectrospray source. Although it may not be explicitly stated, the isotope patterns of all *m*/*z* assignments have been checked by comparison to the calculated theoretical patterns. Single-crystal X-ray diffraction data for **1** and **2** were collected using a Bruker SMART APEX CCD diffractometer at the Technical University of Denmark. Crystals of **3** were examined at the microcrystal diffraction beamline I711 at the MAX-II storage ring, MAXLab, University of Lund, Sweden. All other diffraction data were collected in Odense using a Bruker-Nonius X8 APEX-II instrument. Selected crystallographic data are summarized in Table 1.

(14) The simulation program can be obtained from Dr. H. Weihe, http://sophus.kiku.dk/staff/vip/hogni.html.

(15) (a) van der Sluis, P.; Spek, A. L. *Acta Crystallogr.* **1990**, *A46*, 194. (b) Spek, A. L. *PLATON, A Multipurpose Crystallographic Tool*; Utrecht University: Utrecht, The Netherlands, 2001.

Syntheses. $[Zn_4(dbpbp)Cl_4][Zn_2Cl_6]\cdot EtOH$ (1·EtOH). Dipyridylmethylamine (2.4450 g, 12.33 mmol) dissolved in 20 mL degassed water was added to a cloudy suspension of 4,4′-diphenol (0.3104 g, 1.67 mmol) and *p*-formaldehyde (0.3658 g, 12.18 mmol) in 10 mL degassed EtOH. The resultant yellow suspension was refluxed under N_2 for 3 days to give a dark brown solution and precipitate. After cooling to room temperature, 30 mL H_2O was added to dissolve the precipitate. The aqueous phase was extracted with 5 × 20 mL CH_2Cl_2. and the combined organic phase was dried over anhydrous $MgSO_4$. Removal of the organic phase under reduced pressured gave a dark brown oil, which was chromatographed on a silica column using acetone as eluent to afford a light yellow oil. Crude yield 0.7395 g (43% based on diphenol). The oil was dissolved in EtOH/H_2O, and excess $ZnCl_2\cdot 2H_2O$ (5 g) was added to give light yellow crystals overnight. Yield 0.9655 g (32% based on diphenol). Crystals suitable for X-ray analysis were obtained directly from the mother liquor. ESI-MS (CH_3CN) *m*/*z*: 340.4 ($[Zn_4(dbpbp)Cl_2]^{4+}$, 80%), 465.2 ($[Zn_4(dbpbp)Cl_3]^{3+}$, 100%), 716.3 ($[Zn_4(dbpbp)Cl_4]^{2+}$, 50%). IR (KBr, cm^{-1}): 3436, 2919, 1609, 1574, 1484, 1463, 1443, 1294, 1242, 1157, 1102, 1082, 1054, 1024, 874, 768, 648. Anal. Calcd for $C_{64}H_{60}Cl_{10}N_{12}O_2Zn_6\cdot EtOH$: C, 43.50; H, 3.65; N, 9.22. Found: C, 44.23, H, 3.57; N, 9.28%.

$[Zn_4(dbpbp)(H_2O)(CH_3CN)_3](ClO_4)_6\cdot 2CH_3CN$ (2·2CH₃CN). Recrystallization of **1** from H_2O and CH_3CN in the presence of an excess of $NaClO_4$ yielded **2**·2CH_3CN as pale yellow block-shaped crystals. This product was identified by single-crystal X-ray analysis only.

$[Cu_4(dbpbp)Cl_4][Zn_2Cl_6]\cdot CH_3CN$ (3·CH₃CN). $CuCl_2\cdot 2H_2O$ (117.9 mg, 0.69 mmol) was added to **1**·EtOH (205.9 mg, 0.11 mmol) dissolved in 18 mL warm DMF. After stirring for 15 min at room temperature, CH_3CN was slowly diffused into the dark purple solution yielding green microcrystals overnight. The product was isolated by filtration and washed with small amounts of CH_3CN. Yield 90.7 mg (46% based on **1**·EtOH). Synchrotron single-crystal X-ray analysis was performed on crystals obtained directly from the mother liquor. ESI-MS (DMF) *m*/*z*: 337.9 ($[Cu_4(dbpbp)Cl_2]^{4+}$, 15%), 450.6 ($[Cu_4(dbpbp-H^+)Cl_2]^{3+}$, 30%), 462.7 ($[Cu_4(dbpbp)Cl_3]^{3+}$, 100%), 711.4 ($[Cu_4(dbpbp)Cl_4]^{2+}$, 40%). IR (KBr, cm^{-1}): 3436, 3067, 2868, 2922, 1657, 1610, 1574, 1480, 1461, 1442, 1388, 1288, 1247, 1102, 1052, 1030, 872, 767. Anal. Calcd for $C_{64}H_{60}Cl_{10}Cu_4N_{12}O_2Zn_2\cdot CH_3CN$: C, 44.07; H, 3.53; N, 10.13. Found: C, 43.90; H, 3.76; N, 9.85%.

$[Cu_2Zn_2(dbpbp)(O_2CC_6H_5)_4][Zn_2(O_2CC_6H_5)_2Cl_4]\cdot 4H_2O$ (4·4H₂O). $CuCl_2\cdot 2H_2O$ (31.4 mg, 0.18 mmol) dissolved in 2 mL H_2O was added to **1**·EtOH (147.7 mg, 0.08 mmol) dissolved in 10 mL H_2O and 10 mL acetone. The reaction was heated under reflux for 5 min to give a clear red/brown solution. Sodium benzoate (99.4 mg, 0.71 mmol) was added. After 2 days at room temperature, red crystals of the product were isolated from the solution. Yield 78.5 mg (42% based on **1**·EtOH). Slow evaporation of a CH_3CN solution of **4**·4H_2O afforded crystals suitable for single-crystal X-ray analysis, which were identified as **4**·2CH_3CN. ESI-MS (CH_3CN) *m*/*z*: positive mode 799.5 ($[Cu_2Zn_2(dbpbp)(O_2CC_6H_5)_2Cl_2]^{2+}$, 11%), 842.5 ($[Cu_2Zn_2(dbpbp)(O_2CC_6H_5)_3Cl]^{2+}$, 65%), 886.0 ($[Cu_2Zn_2(dbpbp)(O_2CC_6H_5)_4]^{2+}$, 100%); negative mode 168.8 ($[ZnCl_3]^-$, 100%), 254.8 ($[Zn(O_2CC_6H_5)Cl_2]^-$, 1%). IR (KBr, cm^{-1}): 3435, 3063, 2922, 1609, 1570, 1483, 1463, 1444, 1392, 1291, 1245, 1155, 1052, 1024, 765, 723, 677. UV−vis (CH_3CN) λ_{max}, nm (ϵ, M^{-1} cm^{-1}): 291 (3.0×10^4, sh), 389 (2.1×10^3), 459 (2.0×10^3). Anal. Calcd for $C_{106}H_{90}Cl_4Cu_2N_{12}O_{14}Zn_4\cdot 4H_2O$: C, 53.98; H, 4.19; N, 7.13. Found: C, 53.67; H, 3.80; N, 7.14%.

$[Fe_{0.8}Zn_{3.2}(dbpbp)(O_2CC_6H_5)_4][B(C_6H_5)_4]_{2.8}$ (5). The same procedure as described for **4**·4H_2O was followed using **1**·EtOH (25.0 mg, 0.014 mmol) dissolved in 2 mL acetone, and $Fe(ClO_4)_3\cdot 9H_2O$ (17.7 mg, 0.034 mmol) dissolved in 2 mL H_2O was added. After refluxing for 10 min, the solution was dark green. Upon adding $NaO_2CC_6H_5$ (33.7 mg, 0.240 mmol), a blue/green precipitate formed, which was isolated by filtration and dried in vacuo to yield 21.1 mg crude $[Fe_{0.8}Zn_{3.2}(dbpbp)(O_2CC_6H_5)_4](ClO_4)_{2.8}$ (74% based on **1**·EtOH). ESI-MS (CH_3CN) *m*/*z*: 585.2 ($[Fe_2Zn_2(dbpbp-H)(O_2CC_6H_5)_4]^{3+}$, 35%), 588.5 ($[FeZn_3(dbpbp)(O_2CC_6H_5)_4]^{3+}$, 30%), 618.6 ($[Fe_2Zn_2(dbpbp)(O_2CC_6H_5)_4(ClO_4)]^{3+}$, 80%), 877.7 ($[Fe_2Zn_2(dbpbp-2H^+)(O_2CC_6H_5)_4]^{2+}$, 30%), 883.0 ($[FeZn_3(dbpbp-H^+)(O_2CC_6H_5)_4]^{2+}$, 40%) 887.0 ($[Zn_4(dbpbp)(O_2CC_6H_5)_4]^{2+}$, 30%), 927.4 ($[Fe_2Zn_2(dbpbp-H)(O_2CC_6H_5)_4(ClO_4)]^{2+}$, 85%), 932.3 ($[FeZn_3(dbpbp)(O_2CC_6H_5)_4(ClO_4)]^{2+}$, 70%), 977.8 ($[Fe_2Zn_2(dbpbp)(O_2CC_6H_5)_4(ClO_4)_2]^{2+}$, 100%). Recrystallization from CH_3CN and H_2O with ca. 4 equiv $Na[B(C_6H_5)_4]$ added gave **5** as small green block-shaped crystals.

$[Co_4(dbpbp)(O_2CC_6H_5)_4][B(C_6H_5)_4]_2\cdot x CH_3CN$ (6·xCH₃CN). $Co(ClO_4)_2\cdot 6H_2O$ (1.5 g, 4.1 mmol) and $AgNO_3$ (392.0 mg, 1.7 mmol) were added to **1**·EtOH (302.4 mg, 0.17 mmol) dissolved in 20 mL H_2O and 10 mL acetone. The reaction mixture was refluxed for 3 h, filtered through Celite to remove AgCl, and then refluxed for a further 24 h. After cooling the dark brown solution to room temperature, an excess of sodium benzoate (500 mg, 3.47 mmol) and $NaClO_4\cdot H_2O$ (100 mg, 0.71 mol) dissolved in a minimum of water were added. A dark brown precipitate (which we assume to be a mixture of $[Co_4(dbpbp)(O_2CC_6H_5)_4](ClO_4)_2$ and $[Co_4(dbpbp)(O_2)_2(O_2CC_6H_5)_2](ClO_4)_4$) was filtered off, washed with ice cold water, and redissolved in 40 mL CH_3CN. Insoluble material was removed by filtration through Celite. The solution was degassed, and $H_2NNH_2\cdot H_2O$ (2 mL, 20 M) was added to give a two-phase mixture that changed color from dark brown to light brown upon stirring. The CH_3CN phase was decanted, and 50 mL degassed H_2O was added. A light brown powder precipitated on slow evaporation under N_2. Yield of $[Co_4(dbpbp)(O_2CC_6H_5)_4](ClO_4)_2$ 166.6 mg (46% based on **1**·EtOH). The product is air sensitive and turns dark brown within days. ESI-MS (CH_3CN) *m*/*z*: 376.9 ($[Co_4(dbpbp)(O_2CC_6H_5)_2]^{4+}$, 10%), 535.4 ($[Co_4(dbpbp)(O_2CC_6H_5)_2(ClO_4)]^{3+}$, 30%), 543.0 ($[Co_4(dbpbp)(O_2CC_6H_5)_3]^{3+}$, 75%), 852.7 ($[Co_4(dbpbp)(O_2CC_6H_5)_2(ClO_4)_2]^{2+}$, 10%), 863.8 ($[Co_4(dbpbp)(O_2CC_6H_5)_3(ClO_4)]^{2+}$, 65%), 874.8 ($[Co_4(dbpbp)(O_2CC_6H_5)_4]^{2+}$, 100%). Crystals suitable for single-crystal X-ray analysis were grown by slow evaporation of a CH_3CN solution of $[Co_4(dbpbp)(O_2CC_6H_5)_4](ClO_4)_2$ with 4 equiv $Na[B(C_6H_5)]_4$, from which a few milligrams of pink X-ray quality crystals of **6**·xCH_3CN were isolated.

$[Co_4(dbpbp)(O_2)_2(O_2CC_6H_5)_2](ClO_4)_4$ (7). A few milligrams of **7** were isolated by a method analogous to that for **6** except that 2 equiv sodium benzoate relative to **1** was used in the reaction. ESI-MS (CH_3CN) *m*/*z*: 376.9 ($[Co_4(dbpbp)(O_2CC_6H_5)_2]^{4+}$, 25%), 535.5 ($[Co_4(dbpbp)(O_2CC_6H_5)_2(ClO_4)]^{3+}$, 40%), 546.1 ($[Co_4(dbpbp)(O_2)(O_2CC_6H_5)_2(ClO_4)]^{3+}$, 40%), 556.7 ($[Co_4(dbpbp)(O_2)_2(O_2CC_6H_5)_2(ClO_4)]^{3+}$, 50%), 853.2 ($[Co_4(dbpbp)(O_2CC_6H_5)_2(ClO_4)_2]^{2+}$, 100%). Single crystals suitable for X-ray analysis were not forthcoming.

$[Co_4(bpbp)_2(O_2)_2(BDC)_2](ClO_4)_4\cdot 4(CH_3)_2CO\cdot 8H_2O$ (8). Hbpbp (98.4 mg, 0.18 mmol) dissolved in 4 mL acetone and $Co(ClO_4)_2\cdot 6H_2O$ (125.6 mg, 0.34 mmol) dissolved in 3 mL H_2O were mixed to give a light brown solution. 1,4-Benzenedicarboxylic acid, disodium salt (Na_2BDC) (18.2 mg, 0.09 mmol) in 2 mL H_2O, was added, whereby the solution changed to a dark brown color. Slow evaporation in air at room temperature yielded black crystals of **8** overnight, one of which was used for X-ray diffraction. The remainder were isolated by filtration, washed with small amounts of H_2O and dried in vacuo overnight. Yield 144.0 mg (86% based on $[Co_4(bpbp)_2(O_2)_2(BDC)_2](ClO_4)_4\cdot 6H_2O$). Anal. Calcd for $C_{80}H_{82}$-

Scheme 1. Synthesis of **1**−**7**[a]

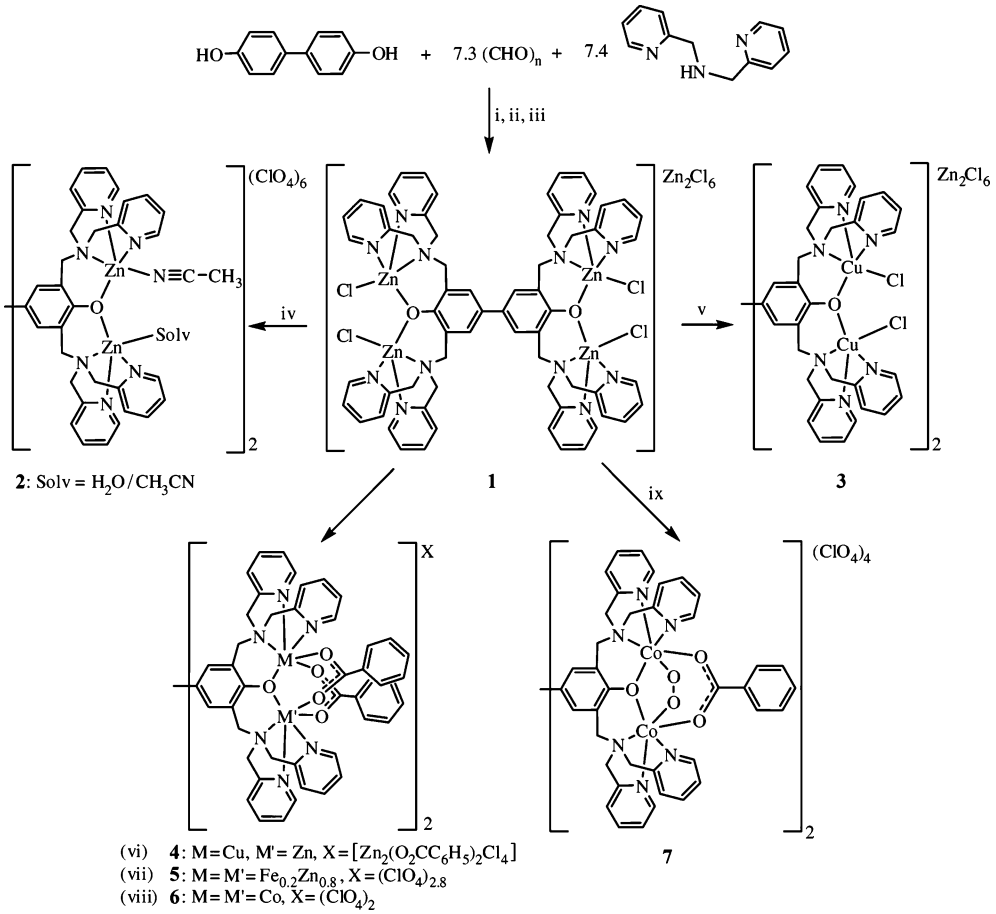

[a] Reagents and reaction conditions follow: (i) EtOH/H_2O (1/2), reflux 3 days; (ii) H_2O, CH_2Cl_2 extraction, chromatography (SiO_2) eluent acetone; (iii) EtOH/H_2O (1/1), excess $ZnCl_2 \cdot 2H_2O$; (iv) recrystallization of **1** in H_2O/CH_3CN with excess $NaClO_4$; (v) 6 equiv $CuCl_2 \cdot 2H_2O$, DMF, diffuse CH_3CN into solution; (vi) 2.2 equiv $CuCl_2 \cdot 2H_2O$, H_2O/acetone (1/1), refluxed 5 min, 9 equiv $NaO_2CC_6H_5$ added, slow evaporation; (vii) same procedure as for **4** but using 2.4 equiv $Fe(ClO_4)_3 \cdot 9H_2O$; (viii) 24 equiv $Co(ClO_4)_2 \cdot 6H_2O$, H_2O/acetone (2/1), 10 equiv $AgNO_3$, reflux 24 h, AgCl removed, excess $NaO_2CC_6H_5$ added, filtered, and redissolved in CH_3CN, added H_2NNH_2, slow evaporation of CH_3CN phase; (ix) same procedure as for **6** except that only ~2 equiv $NaO_2CC_6H_5$ and no H_2NNH_2 was added.

$Cl_4Co_4N_{12}O_{25} \cdot 6H_2O$: C, 45.82; H, 4.52; N, 8.01. Found: C, 45.78; H, 4.25; N, 7.91%. ESI-MS (CH_3CN): *m*/*z* 525.8 ($[\{bpbpCo_2\}_2(BDC)Cl]^{3+}$, 100%), 759.1 ($[bpbpCo_2Cl_2]^+$, 100%), 853.1 ($[\{bpbpCo_2(C_6H_3C_2O_4)\}_3]^+$, 100%).

$[Co_6(bpbp)_3(O_2)_3(BTC)](ClO_4)_6 \cdot 6(CH_3)_2CO$ (9). The same procedure was followed as described for **8**, using Hbpbp (104.8 mg, 0.18 mmol) in 4 mL acetone, $Co(ClO_4)_2 \cdot 6H_2O$ (133.8 mg, 0.36 mmol) in 1 mL H_2O, and 1,3,5- benzenetricarboxylic acid (13.2 mg, 0.06 mmol) dissolved in 2 mL acetone/H_2O, converted into the trisodium salt (Na_3BTC) by addition of 2.5 M NaOH. Tetrahedral crystals of **9** used for X-ray diffraction were taken directly from the reaction mixture. Yield 140.4 mg (74% based on $[Co_6(bpbp)_3(O_2)_3(BTC)](ClO_4)_6 \cdot 8H_2O$). Anal. Calcd for $C_{117}H_{120}Cl_6Co_6N_{18}O_{39} \cdot 8H_2O$: C, 45.15; H, 4.40; N, 8.10. Found: C, 45.04; H, 4.16; N, 7.98%. ESI-MS (CH_3CN): *m*/*z* 379.2 ($[\{bpbpCo_2\}_3(BTC)]^{6+}$, 5%), 396.6 ($[\{bpbpCo_2\}_2(HBTC)]^{4+}$, 100%), 528.4 ($[\{bpbpCo_2\}_2(BTC)]^{3+}$, 100%), 540.4 ($[\{bpbpCo_2\}_2(HBTC)Cl]^{3+}$, 80%), 810.2 ($[\{bpbpCo_2\}_2(BTC)Cl]^{2+}$, 20%), 842.2 ($[\{bpbpCo_2\}_2(BTC)(ClO_4)]^{2+}$, 10%), 897.2 ($[\{bpbpCo_2(HBTC)\}_2]^{2+}$, 20%).

Results and Discussion

Synthesis. The synthesis and initial purification of H_2dbpbp is analogous to the synthesis of Hbpbp,[11] except that 4,4′-diphenol and not 4-*tert*-butylphenol is used as starting material. Chromatographic purification of crude H_2dbpbp on a silica column gives impure oils. Dissolution of the oils in a mixture of H_2O/EtOH in the presence of an excess of $ZnCl_2$ provided a convenient method for extracting the ligand via the preparation of the tetrazinc complex $[(dbpbp)Zn_4Cl_4][Zn_2Cl_6] \cdot$EtOH (**1**·EtOH). Complex **1** could then be used as a starting material for the preparations of $[Zn_4(dbpbp)(H_2O)(CH_3CN)_3](ClO_4)_6$ (**2**), by solvolysis of the terminal chloride ligands, and for $[Cu_4(dbpbp)Cl_4][Zn_2Cl_6]$ (**3**), $[Cu_2Zn_2(dbpbp)(O_2CC_6H_5)_4][Zn_2(O_2CC_6H_5)_2Cl_4]$ (**4**), $[Fe^{III}_{0.8}Zn^{II}_{3.2}(dbpbp)(H_5C_6CO_2)_4][B(C_6H_5)_4]_{2.8}$ (**5**), $[Co_4(dbpbp)(O_2CC_6H_5)_4][B(C_6H_5)_4]_2$ (**6**), and $[Co_4(dbpbp)(O_2)_2(O_2CC_6H_5)_2](ClO_4)_4$ (**7**), by metatheses reactions. These reactions are summarized in Scheme 1.

An almost colorless DMF solution of **1** turns dark purple within minutes after adding roughly 6 equiv $CuCl_2$, indicating the ease by which the four Zn^{II} ions can be completely substituted by Cu^{II}. Green crystals of **3** were isolated by diffusion of CH_3CN into the DMF solutions. Complex **3** produces light red aqueous solutions on dissolution by heating. ESI-MS spectra of these solutions show a base peak at *m*/*z* 329.4, which can be assigned to $[Cu_4(dbpbp)(OH)_2]^{4+}$.

This cation is either present in solution, in which case the hydroxo ligands are likely to form an auxiliary bridge between the two Cu^{II} ions at each end of the $dbpbp^{2-}$ unit,[16] or it is formed in the gas phase by the facile double dehydration of the solution species $[Cu_4(dbpbp)(OH)_2(OH_2)_2]^{4+}$. We have previously observed this latter reaction for related $[M_2(OH)_2(OH_2)_2]^{2+}$ systems.[17] Complexes **1** and **3**, with terminal chloride ligands, proved to be more easily crystallized (and are commensurately more insoluble) than the other $dbpbp^{2-}$ complexes. A probable explanation for this can be found in the solid-state structures, which exhibit intermolecular chloride bridging between Zn^{II} or Cu^{II} ions on adjacent molecules, as described later.

The auxiliary tetracarboxylate-bridged complexes, $[M_4(dbpbp)(O_2CR)_4]^{n+}$, are relatively more difficult to crystallize than **1**, **2**, and **3**. It is evident from the crystal structures of **4** and **5** (described below) that the identity of the counteranion and the specific choice of the auxiliary carboxylate bridge are likely to be critical for successful crystallization of the complexes. The mixed-metal M/Zn complexes were prepared by the reaction of approximately 2 equiv Cu^{II} or Fe^{III} with complex **1** and an excess of benzoate in H_2O/acetone. In the case of the copper-containing reaction, the isolated product is consistent with the stoichiometrically pure mixed-metal red $Cu^{II}_2Zn^{II}_2$ complex **4**, where each phenoxide unit of $dbpbp^{2-}$ bridges between one Cu^{II} and one Zn^{II} center. The specific exchange of only two Zn^{II} for Cu^{II} was confirmed by ESI-MS (base peak *m*/*z* 886.0, assigned to $[Cu_2Zn_2(dbpbp)(O_2CC_6H_5)_4]^{2+}$). In addition, ESR spectroscopy and electrochemistry (see later) indicate that each end of the $dbpbp^{2-}$ unit coordinates specifically one Cu^{II} and one Zn^{II} ion. The reaction was less specific when **1** was reacted under analogous conditions with an Fe^{III} source. The color change clearly indicates exchange of zinc for iron, and ESI-MS spectra of solids reveals $FeZn_3$, Fe_2Zn_2, and Zn_4 ions. The variable Fe^{III}/Zn^{II} distribution is also apparent in the crystal structure of **5**, for which a nonintegral formulation is suggested by the fractional site occupancy of one $[B(C_6H_5)_4]^-$ anion (see below). The bulky nature of the counteranion seems to be critical for successful crystallization, since $[B(C_6H_5)_4]^-$ was the only anion which led to single crystals of **5**. In addition, an unusual dinuclear zinc-benzoate-chloride species, $[Zn_2(O_2CC_6H_5)_2Cl_4]^{2-}$, generated in situ, is present in the crystal lattice of **4**.

As described in the Introduction, the principal metal of interest for this series of complexes is cobalt, since dicobalt complexes of $bpbp^-$ are known to possess reversible O_2-binding properties. However, metathesis reactions of **1** with Co^{II} proved significantly less facile than the reactions with Cu^{II}. The important preparative differences required to achieve Co^{II} substitution are (i) that a large excess of Co^{II} is used, and (ii) that silver nitrate is present to sequester chloride. The Co^{II}_4 system **6** contains two capping *O*,*O*′-bridging benzoate ligands at each terminus, analogous to complexes **4** and **5**. Complex **7** is a Co^{III}_4 system containing one capping bridging benzoate ligand and one capping peroxide ligand at each terminus. The preparative difference between **6** and **7** lies in the large excess of benzoate that was used for **6**. Complex **7** was isolated only in a very low yield, and single crystals suitable for X-ray analysis were not forthcoming. The chemical formulation of **7** was verified by comparison of IR spectra and ESI-MS data with closely related peroxo-carboxylato dicobalt complexes of $bpbp^-$.[13] The ESI mass spectrum of **7** (Figure 2) exhibits dominant quadruply, triply, and doubly charged ions at *m*/*z* 376.9, 535.5, and 853.2, which correspond to the deoxygenated Co^{II} complex, $[Co_4(dbpbp)(O_2CC_6H_5)_2]^{4+}$, and its monoperchlorate and diperchlorate ion pairs, respectively. Observation of these deoxygenated ions is consistent with our previous observations that the gas-phase loss of the mass equivalent to dioxygen is facile.[13] Significantly, comparison of the ESI mass spectra of **6** and **7** demonstrates that the tetrabridged $[Co_4(dbpbp)(O_2CC_6H_5)_4]^{2+}$ cation in **6** is not a contaminant of **7**. Most notable in Figure 2a are two additional triply charged peaks 10.6 and 21.5 *m*/*z* units above the peak for $\{[Co_4(dbpbp)(O_2CC_6H_5)_2](ClO_4)\}^{3+}$, which correspond to the monooxygenated $\{[Co_4(dbpbp)(O_2)(O_2CC_6H_5)_2](ClO_4)\}^{3+}$ (i.e., $\{\mathbf{7} - (O_2) - (ClO_4)_3\}^{3+}$) at the expected *m*/*z* 546.1, and the dioxygenated $\{[Co_4(dbpbp)(O_2)_2(O_2CC_6H_5)_2](ClO_4)\}^{3+}$ (i.e., $\{\mathbf{7} - (ClO_4)_3\}^{3+}$) at the expected *m*/ *z* 556.7. Collision induced dissociation of *m*/*z* 556.7 (Figure 2b) verifies the assignment of $\{\mathbf{7} - (ClO_4)_3\}^{3+}$, since stepwise loss of one, and two, mass equivalents to O_2 (i.e., *m*/*z* 32/3 and 64/3) corresponds to the gas-phase dissociation of one and two neutral dioxygen molecules. The required collision energy is similar to that for O_2 dissociation from $[Co_2(bpbp)(O_2)(O_2CCH_3)]^{2+}$.[13]

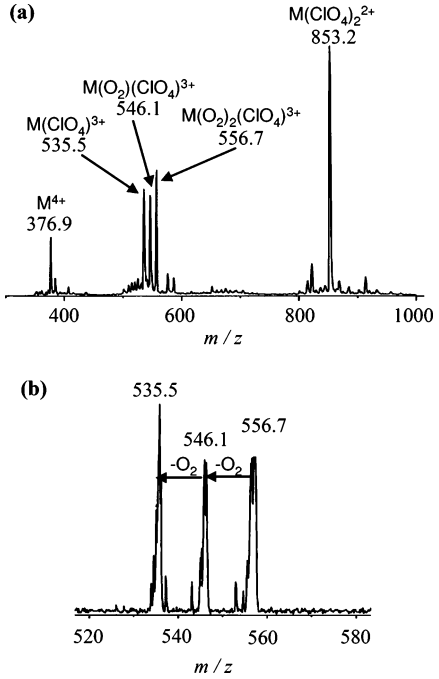

Figure 2. (a) ESI mass spectrum of $[Co_4(dbpbp)(O_2)_2(O_2CC_6H_5)_2](ClO_4)_4$, **7**, M = $\{Co_4(dbpbp)(O_2CC_6H_5)_2\}$. (b) CID spectrum of the peak at *m*/*z* 556.7.

(16) Dalgaard, P.; Hazell, A.; McKenzie, C. J.; Moubaraki, B.; Murray, K. S. *Polyhedron* **2000**, *19*, 1909.
(17) (a) Boisen, A.; Hazell, A.; McKenzie, C. J. *Chem. Commun.* **2001**, 2136. (b) Andersen, U. N.; McKenzie, C. J.; Bojesen, G. *Inorg. Chem.* **1995**, *34*, 1435.

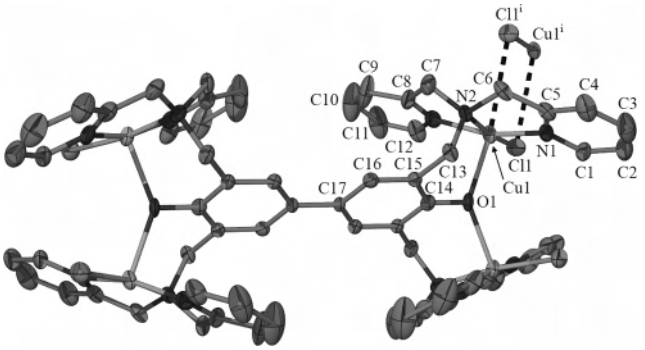

Figure 3. Structure of the $[Cu_4(dbpbp)Cl_4]^{2+}$ cation in **3** showing displacement ellipsoids at 50% probability. H atoms are omitted, and only crystallographically unique atoms are labeled. Black dotted lines indicate intermolecular metal−chloride interactions. The superscript (i) refers to atoms related by the symmetry operator $^1/_2 - x$, $^1/_2 - y$, $^3/_2 - z$. The $[Zn_4(dbpbp)Cl_4]^{2+}$ cation and intermolecular interactions in **1** are comparable.

To establish that the bridging carboxylate ligands BDC and BTC represent viable linkers for the $[Co_4(dbpbp)(O_2)_2]^{6+}$ units, crystallographic characterization was undertaken for the discrete precursor $bpbp^-$ complexes. Reaction of bpbpH, $Co(ClO_4)_2 \cdot 6H_2O$, and 1,4-benzenedicarboxylate in 2:4:1 proportions yields $[Co_4(dbpbp)_2(O_2)_2(C_6H_4C_2O_4)](ClO_4)_4 \cdot 4(CH_3)_2CO \cdot 8H_2O$ (**8**), while the reaction of bpbpH, $Co(ClO_4)_2 \cdot 6H_2O$, and 1,3,5-benzenetricarboxylate in 3:6:1 proportions yields $[Co_6(bpbp)_3(O_2)_3(C_6H_3C_3O_6)](ClO_4)_6 \cdot 6(CH_3)_2CO$ (**9**). These complexes show the expected arrangements of two or three peroxide-carboxylate-bridged dicobalt(III) units around the central BDC or BTC unit (see later).

Crystal Structures. Complexes **1** and **3** are isostructural (Table 1). Crystals of **1** are light yellow or almost colorless, as expected for a Zn^{II} complex, and are formed as large blocks suitable for standard X-ray analysis. Complex **3** forms only very small green block-shaped crystals with the largest dimension being below 0.03 mm, and these crystals were therefore examined using a synchrotron radiation source. The cations of **1** and **3** (Figure 3) display 2/*m* (C_{2h}) point symmetry in the solid state, making one quarter of the cation crystallographically unique. The mirror plane lies perpendicular to the C−C bond connecting the two phenoxide moieties, and the 2-fold rotation axis lies along the C−C bond axis. Each metal ion is pentacoordinated by one chloride and four ligand-based donors: one amine (N_{am}), two pyridine nitrogen atoms (N_{py}), and the bridging phenoxide (O_{ph}). The overall coordination geometry is distorted square-pyramidal, with the M−N_{py} bonds lying trans to each other. The chloride ligands form long intermolecular interactions with metal ions of adjacent molecules (M···Cl = 3.4119(17) and 3.284(3) Å for **1** and **3**, respectively), which can be envisaged to complete a distorted octahedral coordination arrangement. These interactions give rise to a 2-D honeycomb framework structure lying parallel to the $(10\bar{1})$ planes of the unit cell (Figure 4). Within this framework, the hexagon vertices are defined by the phenoxide oxygen, two parallel sides of each hexagon are defined by the biphenoxide group, and the four remaining sides are defined by the intermolecular M···Cl interactions. The hexagonal sheets are

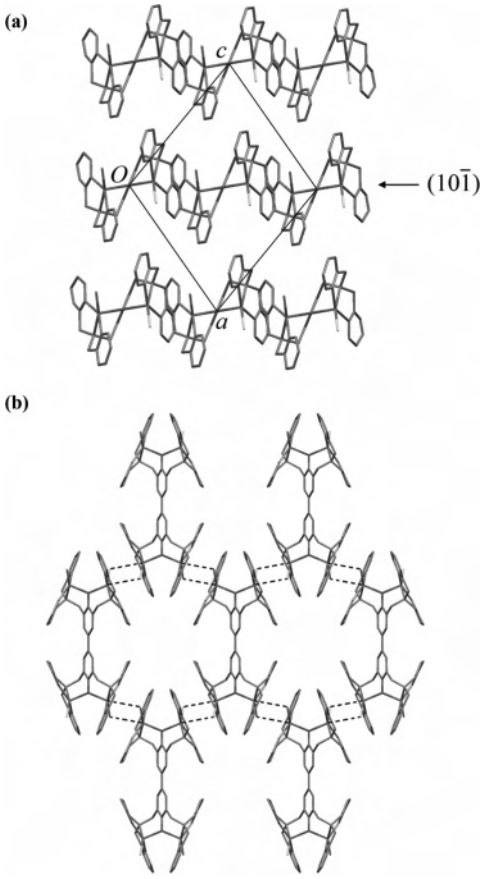

Figure 4. (a) 2-D honeycomb framework structure lying parallel to the $(10\bar{1})$ planes of the unit cell in **3**. Part b shows a single layer in projection. Dashed lines indicate intermolecular M···Cl interactions. Layers are stacked so that the biphenoxide units in one layer lie over the centers of the hexagons in the neighboring layer. H atoms are omitted. The structure of **1** is comparable.

stacked in an ABAB manner, so that the biphenoxide units of the $dbpbp^{2-}$ ligands lie directly above the centers of the hexagons in the adjacent 2-D sheets.

The bond lengths around Zn^{II} in **1** and Cu^{II} in **3** (Table 2) are broadly comparable, except for a slightly shorter Cu−N_{am} distance and a significantly elongated Cu−O_{ph} distance in **3**, which can be attributed to the influence of the Jahn−Teller distortion for Cu^{II}. One consequence of this is a considerably larger Cu···Cu distance in **3** (4.264(3) Å) compared to the Zn···Zn distance in **1** (3.7548(13) Å). The structure of the dinuclear halves of the $[Cu_4(dbpbp)Cl_4]^{2+}$ cation **3** can be compared specifically to the previously reported dinuclear Cu^{II} complex $[Cu_2(bpmp)Cl_2](ClO_4)$.[18] The geometries are closely comparable: the 43 non-H atoms of $[Cu_2(bpmp)Cl_2]^+$ can be superimposed on their counterparts in **3** with an rms deviation of only 0.14 Å. The metal coordination geometry and all metal−ligand bond distances are accordingly comparable, although the Cu···Cu distance in **3** is ca. 0.14 Å larger than 4.128(3) Å in $[Cu_2(bpmp)Cl_2](ClO_4)$. This subtle difference seems likely to stem from crystal packing effects rather than any electronic or geometrical differences between the $bpmp^-$ and $dbpbp^-$ ligands.

(18) Nishida, Y.; Shimo, H.; Maehara, H.; Kida, S. *J. Chem. Soc., Dalton Trans.* **1985**, 1945.

Table 2. Details of the Metal Coordination Geometries (Å) in Complexes **1**−**6**, **8**, and **9**

	1[a]	**2**		**3**[a]	**4**		**5**	
	Zn1	Zn1	Zn2	Cu1	Zn1/Cu1	Zn2/Cu2	Zn1/Fe1	Zn2/Fe2
M···M	3.7548(13)	3.7553(9)		4.264(3)	3.3958(8)		3.352(2)	
M−O_{ph}	2.0331(18)	2.020(4)	2.046(3)	2.269(2)	1.993(3)	2.002(3)	1.998(8)	2.069(8)
M−N_{am}	2.197(4)	2.175(4)	2.175(4)	2.059(6)	2.161(4)	2.169(5)	2.199(11)	2.179(10)
M−N_{py}	2.071(5)	2.067(5)	2.062(4)	1.991(7)	2.087(4)	2.095(4)	2.108(13)	2.094(11)
M−N_{py}	2.084(5)	2.095(5)	2.089(4)	1.997(7)	2.284(5)	2.263(4)	2.133(11)	2.118(12)
M−Cl	2.2681(16)			2.282(2)				
M−$NCCH_3$		2.062(5)	2.066(5)					
M−O_{carb}					1.995(3)	1.989(4)	1.991(10)	2.034(10)
M−O_{carb}					2.193(4)	2.182(4)	2.029(10)	2.101(9)

	6[a]				**8**		**9**	
	Co1	Co2	Co3	Co4	Co1	Co2	Co1	Co2
M···M	3.3880(17)		3.3835(19)		3.1563(12)		3.1625(19)	
M−O_{ph}	2.028(5)	2.018(5)	2.029(7)	2.039(5)	1.901(4)	1.885(4)	1.897(6)	1.895(7)
M−N_{am}	2.135(7)	2.184(5)	2.187(6)	2.194(6)	1.952(6)	2.014(5)	2.030(9)	1.954(8)
M−N_{py}	2.136(7)	2.108(6)	2.143(6)	2.132(7)	1.919(6)	1.901(6)	1.894(10)	1.933(9)
M−N_{py}	2.144(7)	2.157(7)	2.158(4)	2.139(6)	2.008(6)	1.909(5)	1.926(10)	2.004(8)
M−O_{carb}	2.048(6)	2.064(6)	2.048(5)	2.073(5)	1.916(5)	1.917(4)	1.937(7)	1.895(6)
M−O_{carb}	2.110(6)	2.095(5)	2.110(5)	2.149(6)				
M−O_{peroxo}					1.859(5)	1.864(5)	1.860(8)	1.874(6)
O−O					1.410(6)	1.420(9)		

[a] Based on data after application of *SQUEEZE*.[15]

In this regard, it can be noted that $[Cu_2(bpmp)Cl_2](ClO_4)$ also exhibits intermolecular Cu···Cl interactions in the solid state, similar to those in **3**, but that these intermolecular interactions (3.507 Å) are considerably longer than for **3** (3.284(3) Å).

For both **1** and **3**, the $[M_4(dbpbp)Cl_4]^{2+}$ cation is well resolved in the crystal structure, but the counteranion and solvent molecules are not. The counteranions lie in channels running along the *a*-axis and appear to be distributed in a disordered manner within these channels. For **3**, the assignment of Zn rather than Cu in the counteranion is made principally on the basis of the fact that the counteranion does not appear to give a signal in the EPR spectrum (see below). For the synchrotron X-ray data of **3**, it was possible to model (without restraints) an anion that resembled $[Zn_2Cl_6]^{2-}$, disordered by a 90° rotation about an axis that passes through the two bridging Cl atoms. Together with a resolved acetonitrile molecule, also disordered over two orientations, this model provides an acceptable fit to the X-ray data (Table 1). However, the Zn···Zn distance within the $[Zn_2Cl_6]^{2-}$ species is short, and an alternative interpretation of a 4-fold disordered $[ZnCl_4]^{2-}$ anion might also be entertained. In addition, voids of ca. 150 $Å^3$ remain in this structure of **3**, which indicate the presence of further unresolved solvent. Omission of the counteranion and solvent molecules entirely, followed by application of a continuous solvent area model via the *SQUEEZE* program,[15] led to significant improvements in the crystallographic *R*-values and also in the precision of the cationic complex (Table 1). These higher precision values are listed in Table 2 and are used throughout the discussion. The suggested 104 electrons per void in **3** are in better agreement with the 100 electrons expected for $[ZnCl_4]^{2-}$ rather than the 164 electrons expected for $[Zn_2Cl_6]^{2-}$, although the formulation $[Cu_4(dbpbp)Cl_4][Zn_2Cl_6]\cdot CH_3CN$ provides much better agreement with elemental analysis. Similar results were obtained for the X-ray data of **1**, although in this instance it was more difficult to model any chemically reasonable species in the channels along *a*. Satisfactory *R*-factors (R1 ca. 0.08) could be obtained by introducing atoms essentially indiscriminately at peaks in the electron density, but under these circumstances, the continuous solvent area model was preferred. Application of *SQUEEZE* yielded a dramatic improvement (Table 1) and resulted in significantly higher precision for the geometry of the $[Zn_4(dbpbp)Cl_4]^{2+}$ cation (Table 2). In this case, 166 electrons were suggested per void, in better agreement with $[Zn_2Cl_6]^{2-}$, and the formulation $[Zn_4(dbpbp)Cl_4][Zn_2Cl_6]\cdot$ EtOH provides the best fit to the elemental analysis. In the end, the identity of the counteranion and the quantity of the solvent molecules in **1** and **3** remain uncertain. However, the principal points of interest, namely the geometry of the $[M_4(dbpbp)Cl_4]^{2+}$ complex and the formation of the 2-D honeycomb framework via intermolecular M···Cl interactions, are well established by the X-ray results.

The crystal structure of **2** contains the $[Zn_4(dbpbp)(H_2O)(CH_3CN)_3]^{6+}$ cation lying on a center of inversion (Figure 5). In the crystallographically unique half of the complex, one Zn bears a coordinated CH_3CN molecule, while the second appears to bear either CH_3CN or H_2O. From the X-ray data, the CH_3CN molecule in this region is clearly resolved, but refinement with full site occupancy results in displacement parameters for its two C atoms that are significantly larger than that of its N atom. Thus, the CH_3CN molecule was modeled as half-occupied, with a water molecule present otherwise (superimposed on the N atom site). Peaks in the difference density were observed in suitable positions for inclusion as the H atoms of this water molecule. The disordered model gives the uneven formulation $[Zn_4(dbpbp)(H_2O)(CH_3CN)_3]^{6+}$, although the complex exhibits approximate C_{2h} point symmetry, comparable to that of **1** and **3**. The geometrical parameters for the Zn^{II} ions in **2** do not differ significantly from those in **1** (with the

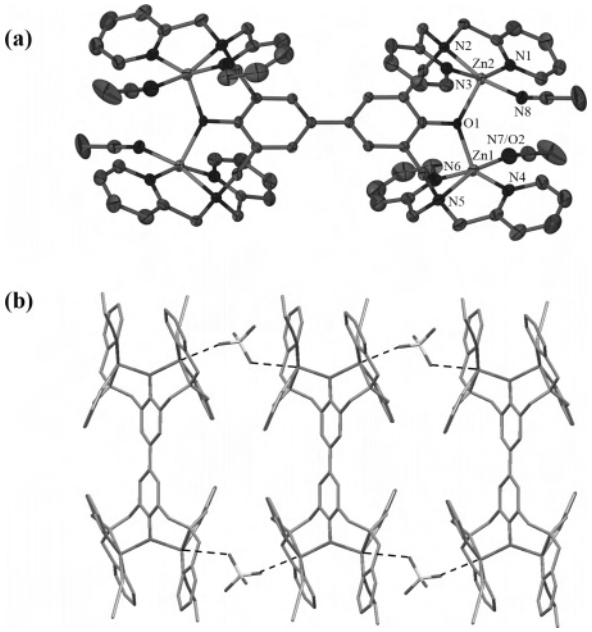

Figure 5. (a) Structure of the $[Zn_4(dbpbp)(H_2O)(CH_3CN)_3]^{6+}$ cation in **2** showing displacement ellipsoids at 50% probability. H atoms are omitted. The terminal ligand coordinated to Zn1 is refined as a disordered mixture of CH_3CN or H_2O with 50/50 site occupancies. (b) Side-on view of a stack of cations, linked through perchlorate anions. Dashed lines denote Zn···O interactions.

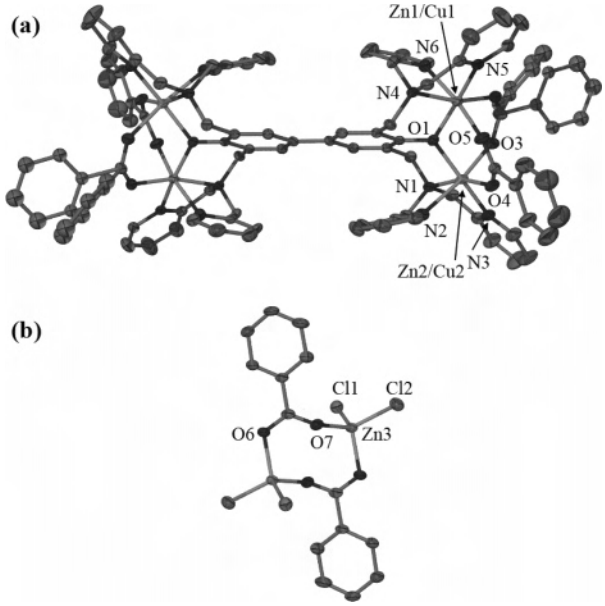

Figure 6. Structure of (a) the $[Cu_2Zn_2(dbpbp)(O_2CC_6H_5)_4]^{2+}$ cation and (b) the $[Zn_2(O_2CC_6H_5)_2Cl_4]^{2-}$ anion in **4**, showing displacement ellipsoids at 50% probability. H atoms are omitted. The $[Fe_{0.8}Zn_{3.2}(dbpbp)(O_2CC_6H_5)_4]^{2.8+}$ cation in **5** is comparable to that shown in part a.

exception of a small contraction of the $Zn-N_{am}$ bond lying trans to the coordinated solvent molecules), and the Zn···Zn distance is 3.7553(9) Å. Complex **2** displays slight asymmetry in its two Zn^{II} coordination environments, with the $Zn1-O_{ph}$ distance of 2.020(4) Å being slightly shorter than the $Zn2-O_{ph}$ distance of 2.046(3) Å. For both unique Zn^{II} ions, a perchlorate anion caps the square face of the pyramidal coordination environment, completing a grossly distorted octahedral arrangement. For Zn1 (which exhibits the CH_3CN/H_2O disorder), the additional $Zn\cdots O_{perchlorate}$ coordination distance is 2.894(5) Å, compared to a much shorter distance of 2.601(4) Å for Zn2. The latter is accompanied by the longer $Zn2-O_{ph}$ distance. The perchlorate anions (containing Cl2) link the molecules via the Zn···O interactions into stacks along the *a*-axis (Figure 5b). Adjacent stacks are relatively loosely packed, with additional perchlorate anions and disordered acetonitrile molecules lying between them.

In the crystal structure of **4**·$2CH_3CN$, both the cation and anion lie on centers of inversion (Figure 6), rendering half of each species unique. The geometry of the cationic complex differs from that in **1**, **2**, and **3** in that the two $M-N_{py}$ bonds in a given metal coordination site lie cis to each other, rather than trans. This results in a V-shaped geometry for each 2-pyridylmethyl arm, rather than the approximately coplanar geometry that is observed in **1**−**3**. This appears to be a direct influence of the presence of the auxiliary benzoate ligand, which completes an approximately octahedral coordination environment for each metal ion. Although ESI mass spectra reveal only Zn_2Cu_2 cations, therefore suggesting a strict stoichiometric system, there is no significant difference in coordination for the two independent metal sites in the cation (Table 2). Both metal sites were therefore refined as an equal mixture of Cu^{II} and Zn^{II}. The lack of detectable $Cu^{II}-Cu^{II}$ interactions in the EPR spectra, as well as in cyclic voltammetry experiments (see below), indicate that each half of the $dbpbp^{2-}$ ligand actually binds specifically one Cu^{II} and one Zn^{II}, so that the formulation of the cation could be written more precisely as $[(C_6H_5CO_2)_2CuZn(dbpbp)CuZn(O_2CC_6H_5)_2]^{2+}$. The X-ray results suggest that these metal sites do not exhibit long-range order in the solid state. The benzene ring of one benzoate unit bridging the metal sites also exhibits disorder in the crystal structure, and this was refined over two positions with 65% and 35% site occupancy. The disordered interpretation is supported by the solid-state EPR spectrum which indicates the presence of two distinct Cu^{II} environments in a 1:2 ratio (see below). The counteranion, $[Zn_2(O_2CC_6H_5)_2Cl_4]^{2-}$ (Figure 6b), was identified clearly in the structural analysis, although with both Cu^{II} and Zn^{II} present in the system, the metal cannot be identified uniquely from the X-ray data alone. The assignment as Zn rather than Cu is supported by ESI-MS, which identifies appropriate fragment ions $[Zn(O_2CC_6H_5)Cl_2]^-$ m/z = 254.8 and $[ZnCl_3]^-$ m/z =168.8. The anionic species $[Zn_2(O_2CC_6H_5)_2Cl_4]^{2-}$ bears a close geometrical resemblance to the previously reported neutral complex $[Nb_2(O_2CC_6H_5)_2Cl_4(OEt)_4]$,[19] in which each Nb^V ion attains octahedral coordination through additional EtO^- ligands.

Although the crystal of **5** was relatively weakly diffracting (ca. 55% data observed at the $2\sigma(I)$ level to a resolution of 1.0 Å), the cationic complex and one independent $[B(C_6H_5)_4]^-$ counteranion were well resolved. However, a second independent $[B(C_6H_5)_4]^-$ anion displayed significantly enlarged displacement ellipsoids, indicative of partial site occupancy. The situation was modeled as follows: (1) the poorly

(19) Brown, D. A.; Wallbridge, M. G. H.; Li, W.-S.; McPartlin, M.; Scowen, I. J. *Inorg. Chim. Acta.* **1994**, *227*, 99.

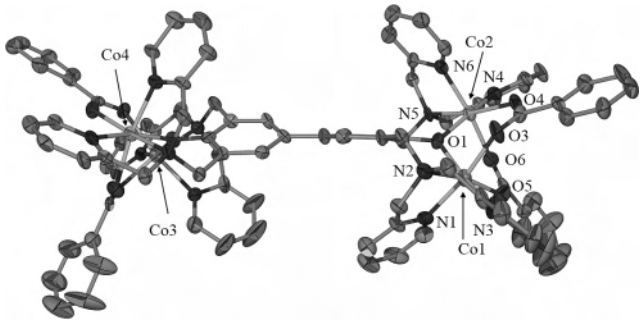

Figure 7. Structure of the $[Co_4(dbpbp)(O_2CC_6H_5)_4]^{2+}$ cation in **6** showing displacement ellipsoids at 50% probability. H atoms are omitted. The complex exhibits a twist about the central C−C bond in the biphenoxide unit.

resolved $[B(C_6H_5)_4]^-$ anion was included with all phenyl rings constrained to be hexagonal and the overall geometry restrained to be comparable to that of the well-resolved $[B(C_6H_5)_4]^-$ anion; (2) the displacement parameters of the fractional $[B(C_6H_5)_4]^-$ anion were fixed at 0.12 Å^2 (comparable to those of the well-resolved $[B(C_6H_5)_4]^-$ anion), and the site occupancies were refined as a single common value, giving 0.386(6); (3) the site occupancy factors were then constrained to be 0.4 (a moderate approximation to simplify the empirical formula), and a single isotropic displacement parameter common to all atoms in the partially occupied $[B(C_6H_5)_4]^-$ anion was refined, giving an acceptable value of 0.167(5) Å^2. The fractional description of the second $[B(C_6H_5)_4]^-$ anion results in a total of 2.8 $[B(C_6H_5)_4]^-$ anions per cation. Charge balance requires that the positive charge on the metal ions sums to 8.8+, leading to an average formulation of $[Fe^{III}_{0.8}Zn^{II}_{3.2}(dbpbp)(O_2CC_6H_5)_4]^{2.8+}$. This formulation provides only a relatively crude approximation, averaged over the entire crystal.

The cationic complex in **5** lies on a center of inversion in the solid state, rendering the two halves of the cation crystallographically equivalent. As for **4**, the Fe/Zn−N_{py} bonds lie in a cis arrangement, but in this case there is a discernible difference between the coordination geometries of the two unique metal sites (Table 2). In particular, one site displays a significantly shorter Fe/Zn−O_{ph} distance, and a moderate contraction of one Fe/Zn−O distance to one bridging benzoate group. The asymmetry in the coordination geometries of the metal ion sites suggests that the Fe1/Zn1 site may be relatively richer in the smaller Fe^{III} ion, although the relatively low precision of the crystal structure does not warrant any significant conclusions in this regard, and a uniform $Fe^{III}_{0.2}Zn^{II}_{0.8}$ distribution was modeled for both metal sites. The disordered interpretation is supported by ESI-MS results, in which $FeZn_3$, Fe_2Zn_2, and Zn_4 ions are observed in the gas phase. Where the fractionally occupied $[B(C_6H_5)_4]^-$ anion is absent in the solid state, the resulting voids are likely to be occupied by acetonitrile solvent molecules, which are not expected to be resolved.

Complex **6** is crystallographically distinct among the set in that it lies on a general position in the crystal structure, rendering all Co^{II} sites independent (Figure 7). Reduction of the symmetry of the $[Co_4(dbpbp)(O_2CC_6H_5)_4]^{2+}$ cation arises as a result of a small twist about the central C−C bond in the biphenoxide unit of $dbpbp^{2-}$, giving a dihedral angle of 29.4(3)° between its two benzene rings. This must be attributed to crystal packing effects. The coordination environments of the four Co^{II} ions are comparable (Table 2), the only significant differences being a small contraction of one Co1−N_{am} distance compared to its counterparts for Co2, Co3, and Co4, and slight elongation of one Co4−O distance to one bridging benzoate. Complex **6** is the first reported carboxylate-bridged $bpbp^-$, $bpmp^-$, or $dbpbp^-$ system containing Co^{II} (all previously reported examples have contained Co^{III}), so that there are no reported structures available for comparison. The coordination distances around Co^{II} are similar to those in the Zn^{II} analogues (Table 2), although the cis arrangement of the M−N_{py} bonds in **6** contrasts with that in the non-carboxylate-bridged **1**, **2**, and **3**. On average, the Co^{II}−O_{ph} distances in **6** are ca. 0.13 Å longer than those in the Co^{III} complexes **8** and **9**, the Co^{II}−N_{am} distances are ca. 0.19 Å longer, and the Co^{II}−N_{py} distances are ca. 0.14 Å longer. Although the two halves of the $[Co_4(dbpbp)(O_2CC_6H_5)_4]^{2+}$ cation are twisted with respect to each other in **6**, the gross geometry of each half is comparable to that in **5**. In addition, the $[B(C_6H_5)_4]^-$ anions occupy similar positions with respect to the cations in both **5** and **6**, adjacent to the central biphenoxide unit and involved in edge-to-face C−H$\cdots\pi$ interations with it.

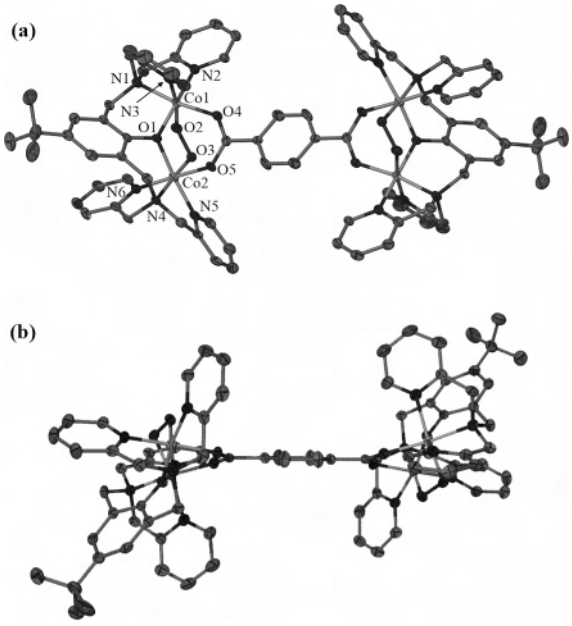

Figure 8. Perpendicular views of the $[Co_4(bpbp)_2(O_2)_2(BDC)]^{4+}$ cation in **8** showing displacement ellipsoids at 50% probability. H atoms are omitted.

The cationic complex in **8** (Figure 8) lies on a crystallographic center of inversion, rendering the two dinuclear $[Co_2(bpbp)(O_2)]^{3+}$ units equivalent. The two peroxo bridges lie on either side of a plane defined by the BDC^{2-} unit (Figure 8b), and the O−O distance of 1.410(6) Å is typical for this type of peroxo bridge.[13a,20] The geometry of each $[Co_2(bpbp)_2(O_2)]^{3+}$ unit in **8** is closely comparable to that of the structurally characterized dinuclear Co^{III} complex

(20) Suzuki, M.; Ueda, I.; Kanatomi, H.; Murase, I. *Chem. Lett.* **1983**, 185.

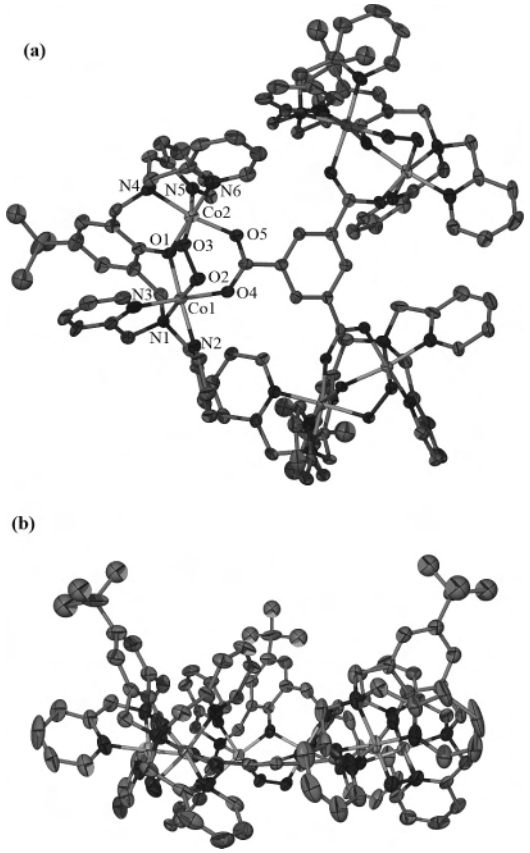

Figure 9. Perpendicular views of the $[Co_6(bpbp)_3(O_2)_3(BTC)]^{6+}$ cation in **9** showing displacement ellipsoids at 50% probability. H atoms are omitted.

$[Co_2(bpbp)(O_2)(O_2CCH_3)]^{2+}$:[13a] the 46 non-H atoms (excluding the *tert*-butyl groups and CH_3/benzene groups of the acetate/benzoate bridges) can be superimposed with a total rms deviation of 0.21 Å. The two independent Co^{III} coordination sites in **8** are different. For Co1, the $Co-O_{peroxo}$ bond lies trans to one $Co-N_{py}$ bond, and the latter is elongated compared to the other three unique $Co-N_{py}$ bonds. For Co2, the $Co-N_{am}$ bond lies trans to the peroxo bridge, and this exhibits similar elongation. The same effect is observed in the isolated complex $[Co_2(bpbp)(O_2)(O_2CCH_3)]^{2+}$.[13a] Linking of the two $[Co_2(bpbp)_2(O_2)]^{3+}$ units via the BDC^{2-} group therefore has no significant influence on the geometry of the dinuclear units, and we would expect no significant influence on the O_2 binding properties. The *tert*-butyl groups of the $bpbp^-$ ligands project to either side of the plane of the BDC^{2-} unit, and the central phenoxide ring of each $bpbp^-$ unit forms a dihedral angle of 46.8(4)° with it. Thus, in the context of our envisaged construction of network polymers, the $[Co_4(bpbp)_2(O_2)_2(BDC)]^{4+}$ cation constitutes a "zigzag" linker unit rather than a planar one.

Compound **9** crystallizes in a cubic space group, with the $[Co_6(bpbp)_3(O_2)_3(BTC)]^{6+}$ cation (Figure 9) lying on a 3-fold rotation axis, so that each of its three dinuclear $[Co_2(bpbp)(O_2)]^{3+}$ units are crystallographically equivalent. In this case, all three peroxo groups lie on the same side of the plane defined by the BTC unit (contrary to the cation in **8**), and the O−O distance of 1.420(9) Å does not differ significantly from that in **8**. The geometry of the $[Co_2(bpbp)(O_2)]^{3+}$ unit as a whole is also entirely comparable to that in **8**: the appropriate 46 non-H atoms in **8** and **9** can be superimposed with an rms deviation of only 0.20 Å. Thus, linking of the $[Co_2(bpbp)(O_2)]^{3+}$ units via the BTC^{3-} group is shown to have no significant influence on the geometry of the dinuclear units, so that again we would expect no significant influence on the O_2 binding properties. The dihedral angle between the plane of the BTC^{3-} unit and the phenoxide ring within each $bpbp^-$ ligand is 70.5(5)°. Thus, the complex as a whole adopts a "bowl-shaped" conformation in which the *tert*-butyl groups of the $bpbp^-$ ligands project to the same side of the plane containing the BTC^{3-} group (Figure 9b).

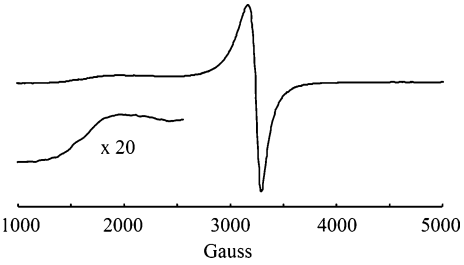

Figure 10. X-band EPR spectrum of a powdered sample of **3**·$4H_2O$ at 116 K (microwave power 2.0 mW, modulation amplitude 1 mT, modulation frequency 100 kHz, sweep rate 11.9 mT s^{-1}).

EPR Spectroscopy and Electrochemistry of the Copper Complexes. The EPR spectrum of a powdered sample of **3** at 116 K (Figure 10) shows an asymmetric broad unresolved resonance at $g = 2.09$ ($\Delta M_s = \pm 1$ transitions) and a very weak resonance at half field $g \approx 4.1$ ($\Delta M_s = \pm 2$ transition for a coupled $S = 1$ state), indicative of dipolar and weak exchange coupling between Cu^{II} ions.[16,21] Coupling interactions are potentially complicated by plausible one-atom intramolecular superexchange pathways via the bridging phenoxide oxygen atom, and intermolecular pathways via the chloride bridges to Cu^{II} ions in adjacent molecules.

By contrast, the solid-state EPR spectrum of a powdered sample of **4**·$2CH_3CN$, at 116 K (Figure 11a), indicates uncoupled Cu^{II} ions. The spectrum shows two overlapping axial Cu^{II} signals in the $g = 2$ region. A simulated spectrum for each Cu^{II} species was calculated[14] with the parameters given in Table 3. A combination of the two simulated spectra in a 2:1 ratio (67% major component + 33% minor component) gave the best fit to the experimental data (Figure 11a). This is in agreement with the X-ray analysis, which suggested a disordered benzoate occupying two different positions with 65% and 35% site occupancies. Thus, although the differences in coordination environment appear to be small on the basis of the X-ray data, EPR data clearly show that the disorder of the benzoate ligand gives two different coordination environments around Cu^{II}. This difference is shown to be confined to the solid state by the EPR spectrum of **4** in CH_3CN solution (∼5 mM) at 116 K (Figure 11b), which shows only one type of Cu^{II} ion. The *g* values used to simulate the spectrum are exactly an average of the *g* values for the two components used to simulate the powder spectrum (Table 3).

(21) Klingele, J.; Moubaraki, B.; Murray, K. S.; Boas, J. F.; Brooker, S. *Eur. J. Inorg. Chem.* **2005**, *8*, 1530.

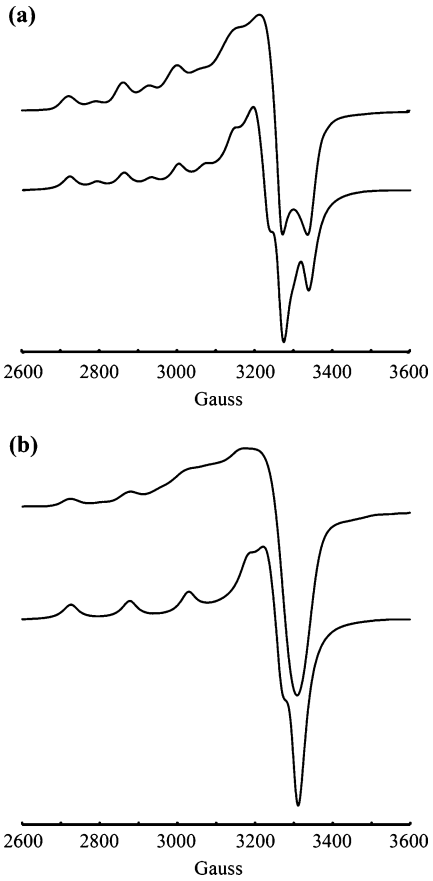

Figure 11. X-band EPR spectra of **4**·4H_2O at 116 K as (a) a powdered sample and (b) a frozen CH_3CN solution (~5 mM). In both parts, the experimental spectrum is on top (microwave power 2.0 mW, modulation amplitude 1 mT, modulation frequency 100 kHz, sweep rate 11.9 mT s^{-1}, average of 10 scans), and the simulated spectrum is on the bottom (computed using the parameters from Table 3).

Table 3. EPR Spin-Hamiltonian Parameters for **4**

	powder sample at 116 K		
	major component	minor component	frozen glass in CH_3CN at 116 K
$g_{\|\|}$	2.3085	2.256	2.290
$g_\perp$	2.099	2.056	2.075
$A_{\|\|}$ (cm^{-1})	0.0151	0.0146	0.0162
$A_\perp$ (cm^{-1})	0.001	0.001	0.001
line width (G)	28.0	28.0	28.0
ν(GHz)	9.476	9.476	9.467

One reduction peak in the cyclic voltammogram of **4** (Figure 12) supports the suggestion that the two Cu^{II} ions are isolated on either side of the $dbpbp^-$ ligand. One broad irreversible cathodic peak is observed at $E_{pc} = -1.42$ V when scanning from −0.39 to −2 V, corresponding to the formation of Cu^I. Previous electrochemical studies of $[Cu_2(bpmp)(OH_2)_2](ClO_4)_3$·4$H_2O$[22] have shown two one-electron reductions ($Cu_2^{II,II}/Cu_2^{II,I}$ reversible and $Cu_2^{II,I}/Cu_2^{I,I}$ irreversible). Since only one reduction peak appears for **4**, the two Cu^{II} ions must be equivalent and hence not coordinated on the same side of the $dbpbp^{2-}$ ligand. The irreversibility of the peak at −1.42 V indicates rapid decomposition of Cu^I-

(22) Torelli, S; Belle, C.; Gautier-Luneau, I.; Pierre, J. L.; Saint-Aman, E.; Latour, J. M.; Le Pape, L.; Luneau, D. *Inorg. Chem.* **2000**, *39*, 3526.

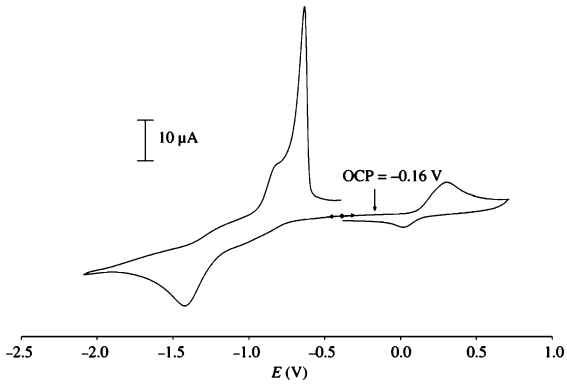

Figure 12. Cyclic voltammogram for a 4.3 mM solution of **4**·4H_2O in 0.1 M TBAP in CH_3CN vs $Fc^{+/0}$, scans between −0.39 and 0.71 V and then between −0.39 and −2.09 V.

Scheme 2. Conceptual Combination of the Structurally Characterized Units **7**, **8**, and **9** To Produce (a) a 1-D Linear Polymer with Stoichiometry $[\{Co_4(dbpbp)(O_2)_2(BDC)\}_n]^{4n+}$ and (b) a 2-D Honeycomb Framework with Stoichiometry $[\{Co_4(dbpbp)(O_2)_2(BTC)_{[2/3]}\}_n]^{4n+}$ [a]

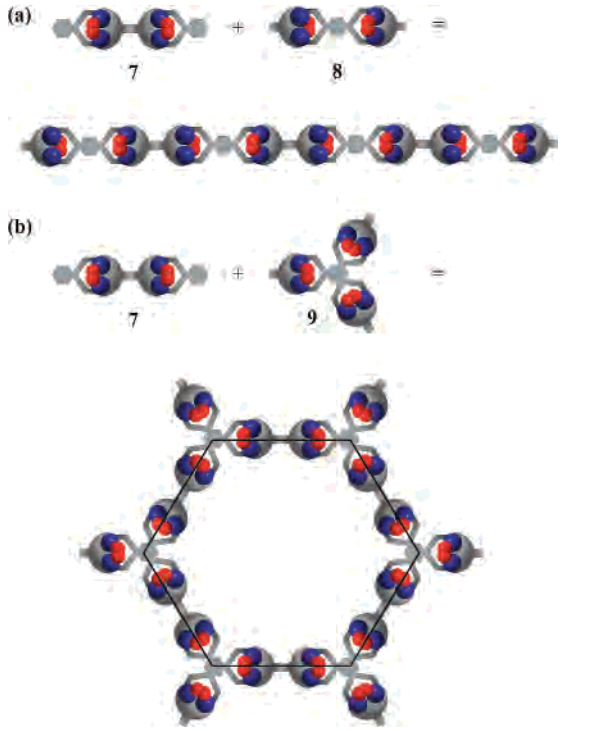

[a] The dark spheres represent Co^{III} ions, and the lighter spheres, oxygen atoms. The scheme illustrates only 2-D projections, although nonplanarity or 3-D networks could arise.

Zn^{II}, while the sharp oxidative peak at $E_{pa} = -0.64$ V is characteristic of redissolution of Cu^0 formed on the electrode on reduction of Cu^I released from the ligand. The release of Cu^I might also induce further substitution of Zn^{II} in **4** to generate $\{Cu_3Zn(dbpbp)\}$ or $\{Cu_4(dbpbp)\}$ complexes. The weak shoulder at $E_{pa} = -0.84$ V could therefore be oxidation of $Zn^{II}Cu^{II}(dbpbp)Cu_2^{II,I}$ or $Cu_2^{II,I}(dbpbp)Cu_2^{II,I}$ species formed near the electrode surface. Positive scans from −0.39 to 0.71 V show one anodic peak, at $E_{pa} = 0.29$ V, and one cathodic peak at $E_{pc} = 0.03$ V.

Toward the Production of Coordination Polymers/MOFs. As stated in the Introduction, characterization of complexes **1**−**9** represent our preliminary steps toward the potential production of coordination polymers/MOFs that

incorporate functional dimetallic units. On the basis of the preceding discussion, a suitable strategy for construction of coordination polymers is exemplified by Scheme 2. Conceptual combination of the complex $[Co_4(dbpbp)(O_2)_2(O_2CC_6H_5)_2]^{4+}$ (**7**) with the cation $[Co_4(bpbp)_2(O_2)_2(BDC)]^{4+}$ (**8**) would lead to construction of 1-D chains. In practice, this amounts to the synthesis described for **7** with BDC^{2-} present in place of benzoate. Similarly, conceptual combination of $[Co_4(dbpbp)(O_2)_2(O_2CC_6H_5)_2]^{4+}$ and the cation $[Co_6(bpbp)_3(O_2)_3(BTC)]^{6+}$ (**9**) might be expected to yield 2-D honeycomb sheets of stoichiometry $[Co_4(dbpbp)(O_2)_2(BTC)_{2/3}]_n^{4n+}$, or potentially 3-D networks if, for example, there should be rotation around the axes of the links between the 3-connecting nodes. Practically, the preparation amounts to the synthesis described for **7** with BTC^{3-} present in place of benzoate. Incorporation of a tetrahedral tetracarboxylate node such as adamantane-1,3,5,7-tetracarboxylate could also be envisaged to produce 3-D polymers/MOFs. Our initial attempts at polymer formation certainly produce isolable solids that are polymeric in character. However, in the absence of long-range three-dimensional order, we have so far been unable to characterize these products uniquely (i.e., by X-ray diffraction).

Conclusion

The structures of the tetranuclear complexes reported here demonstrate the potential of the new tetranucleating ligand $dbpbp^{2-}$ for construction of coordination polymers/MOFs that contain enzymelike dimetallic substrate binding sites. Homometallic M_4 and heterometallic $M_2M'_2$ systems have been shown to be accessible for $dbpbp^{2-}$, and the structures of these systems resemble closely those of functional homo- and heterometallic dinuclear complexes known for the parent ligands $bpmp^-$ and $bpbp^-$. Thus, we would not expect any loss of functionality as a result of incorporating these units into the envisaged coordination polymers/MOFs. So far, we have prepared the $dbpbp^{2-}$ complexes by metathesis reactions of the Zn_4 complex, which initially provided the most convenient means to isolate the $dbpbp^{2-}$ ligand. As a result, complexes have been accessible only for metal ions able to displace Zn^{II} from $dbpbp^{2-}$. In the case of Fe^{III}, this led to incomplete substitution to form a nonstoichiometric Fe^{III}/Zn^{II} system, and the preparation of our principal target Co^{II}_4 complexes required large excesses of Co^{II} to displace all four Zn^{II} ions. To permit more convenient and controlled preparation of these metal complexes, future work will prioritize isolation of the pure protonated ligand, H_2dbpbp.

On the path toward production of functional BDC- and BTC-connected $[Co_4(dbpbp)(O_2)_2]^{6+}$-based coordination polymers/MOFs, the structures of the tetra- and hexanuclear cations containing BDC- and BTC-linked $[Co_2(bpbp)(O_2)]^{3+}$ units provide an indication of the geometrical features of these potential nodal points. Our initial attempts to prepare such polymers have yielded insoluble solid materials consistent with polymer formation, but progress toward unambiguous characterization of these products has so far been hindered by unsuccessful crystallization attempts. Crystallization of these materials will be essential, since X-ray structure determination provides the only reliable method for characterization of systems of this type. Preparation in much larger quantities is desirable. We are then hopeful that manipulation of preparative factors, for example the order of reactant addition and the choice of appropriate counteranions, will facilitate crystallization, and we are proceeding in this direction.

Acknowledgment. This work was supported by the Danish Technical and Natural Science Research council (Grant 26-02-0192). We are grateful to Drs. Inger Søtofte and Niels Thorup at the Technical University of Denmark for access to the Bruker SMART X-ray diffractometer in Lyngby. We thank the Danish Natural Science Research Council and Carlsbergfondet for provision of the X-ray equipment in Odense and for funding to ADB via a STENO stipend (Grant 21-03-0164).

Supporting Information Available: Crystallographic data (CIF) for the eight reported structures, including both conventional and *SQUEEZE* refinement of **3**. This material is available free of charge via the Internet at http://pubs.acs.org.

IC062131S